Simultaneous Measurement of Urban and Rural Single Particles in Beijing, Part I: Chemical Composition and Mixing State

Yang Chen[1], Jing Cai[2], Zhichao Wang[1], Chao Peng[1], Xiaojiang Yao[1], Mi Tian[1], Yiqun Han[2], Guangming Shi[1,3], Zongbo Shi[4,5], Yue Liu[2], Xi Yang[2], Mei Zheng[2*], Tong Zhu[2], Kebin He[6], Qiang Zhang[7], and Fumo Yang[3,1*]

[1]Center for the Atmospheric Environment Research, Chongqing Institute of Green and Intelligent Technology, Chinese Academy of Sciences, Chongqing 400714, China

[2] SKL-ESPC and BIC-ESAT, College of Environmental Sciences and Engineering, Peking University, Beijing 100871, China

[3]College of Architecture and Environment, Sichuan University, Chengdu 610065, China

[4] School of Geography Earth and Environmental Sciences, University of Birmingham, Birmingham B15 2TT, UK

[5]Institute of Surface-Earth System Science, Tianjin University, Tianjin 300072, China

[6] School of Environment, Tsinghua University, Beijing 100084, China

[7]Department of Earth System Science, Tsinghua University, Beijing, China

Corresponding to Fumo Yang (fmyang@scu.edu.cn) and Mei Zheng (mzheng@pku.edu.cn)

Keywords: urban; regional; single particle; transport; mixing state

Abstract

Two single particle aerosol mass spectrometers (SPAMS) were deployed simultaneously at an urban and a rural site in Beijing during an intensive field campaign from 1st to 29th Nov 2016 to investigate the source and process of airborne particles in Beijing. In the first part of this research, we report the single-particle chemical composition, mixing state, and evolution at both sites. 96% and 98% of collected particles were carbonaceous at the urban and rural sites, respectively. Five particle categories, including elemental carbon (EC), organic carbon (OC), internal-mixed EC and OC (ECOC), potassium-rich (K-rich), and Metals were observed at both sites. The categories were partitioned into particle types depending on different atmospheric processing stages. Seventeen particle types were shared at both sites. In the urban area, nitrate-containing particle types, such as EC-Nit and ECOC-Nit, were enriched, especially at night; sulfate-containing particles were transported when wind speed was high; ECOC-Nit-Sul were mostly local-aged. In sum, these processed particles took up to 85.3% in the urban areas. In the rural area, regional particles were abundant, but freshly emitted ECOC and OC had distinct patterns that were pronounced at cooking and heating time. Biomass burning, traffic, and coal burning were major sources of $PM_{2.5}$ in both rural and urban areas. Besides, the particles from the steel industry located in the south were also identified. In summary, the chemical composition of urban and rural particle types was similar in Beijing; the urban particles were influenced significantly by rural processing and transport. The work is useful to understand the evolution of urban and rural particles in Beijing during winter.

1. Introduction

China has experienced severe haze events caused by extremely high concentrations of fine particulate matter ($PM_{2.5}$) since January 2013. In the worst cases, an area of 2.0 million km^2 and a population of 800 million were affected (Huang et al., 2014). In the Beijing-Tianjin-Hebei (BTH) area, extreme haze events frequently occur during winter, with $PM_{2.5}$ mass reaching rapidly up to 200 μg m^{-3} and sustaining such levels for hours (Guo et al., 2014).

Over the last two decades, comprehensive studies have been conducted on urban PM in Beijing. He et al. (2001) reported the first characterization of $PM_{2.5}$. Since then, numerous studies have been published on characterization (Huang et al., 2010), sources (Guo et al., 2012; Sun et al., 2014a), and processing of PM (Sun et al., 2013). The mechanism of rapid-boosting $PM_{2.5}$ in Beijing, including new particle formation and growth (Guo et al., 2014), regional transport (Li et al., 2015), and both (Du et al., 2017; Sun et al., 2014a), have been proposed. However, discrepancies remain among these studies. For example, the mass loading of $PM_{2.5}$ can rapidly increase to hundreds μg m^{-3}. Both Wang et al. (2016) and Cheng et al. (2016) suggested the secondary formation of sulfate from the oxidation of NO_2, while (Guo et al., 2014) proposed a mechanism of particle formation and growth. Different from local secondary formation and accumulation, Li et al. (2015) proposed that particles via long-range transport cause the elevation of $PM_{2.5}$. According to Sun et al. (2014b) and Zhai et al. (2016), regional transport plays an important role during heavy haze episodes. However, most studies have focused on the urban areas of Beijing, with limited

attention paid to rural areas. To illustrate the sources, evolution, and transport of particles, the investigation of rural areas around Beijing is necessary.

Single particle mass spectrometers (SPMS) have been used to investigate the size-resolved chemical composition and mixing state of atmospheric particles (Gard et al., 1997; Pratt and Prather, 2012). More recently, single particle aerosol mass spectrometers (SPAMS) have been used in Chinese megacities such as Beijing (Li et al., 2014), Shanghai (Tao et al., 2011), Guangzhou (Bi et al., 2011), Xi'an (Chen et al., 2016; Chen et al., 2019a), Nanjing (Wang et al., 2015), and Chongqing (Chen et al., 2017). SPAMS has been proven a useful tool for characterizing the single-particle chemical composition, mixing state, and processing of atmospheric particles. Due to the nature of laser desorption/ionization (LDI), the instrument is very sensitive to dust and other types of particles containing sodium and potassium, and this may cause bias in the particle matrix (Pratt and Prather, 2012).

In Beijing, particle types, such as carbonaceous, metal, dust, K-rich, and others during spring and fall, were reported (Liu et al., 2016b; Li et al., 2014). Besides, lead-containing particles have also been investigated in recent studies (Ma et al., 2016; Cai et al., 2017). Organics, sulfate, nitrate, ammonium and other species have been found internally mixed in the atmospheric particles, and these particle types are mostly from the combustion of fuel or biomass. The abundance of secondary species can indicate the degree of aging during atmospheric processing. Particles are with more secondary species with deeper processing. However, these studies lack the use of this data to provide a view of the dynamic particulate processing. Therefore, we used the relative abundance of secondary species to adequately illustrate the process of single particles at both sites, providing a tracing system on a regional scale.

This study is a part of the APHH-Beijing (Atmospheric Pollution and Human Health in a Chinese Megacity of Beijing) intensive field campaign during winter 2016 (Shi et al., 2019). Two SPAMSs were deployed simultaneously at Peking University (PKU) and Pinggu (PG) in order to observe both urban and rural particles in the Beijing region. The aims of the study are 1) to characterize the single-particle chemical composition and mixing state; 2) to investigate particulate evolution at both sites during haze events. These two objectives are presented in two parts. In Part I, particle types and their atmospheric processing (e.g., origination, source, and diurnal profiles) at both sites are reported; in Part II, the detailed analysis of haze events, effects of heating activities, and evidence of regional transport are addressed.

2. Methodology

2.1 Sampling sites

The campaigns were performed simultaneously at PKU (116.32ºE, 39.99ºN) and PG (117.05ºE, 40.17ºN) from 11/01/2016 to 11/29/2016. A Description of the PKU site is available in the literature (Huang et al., 2006). Briefly, the site is located on the rooftop (15 m above the ground) on the PKU campus which is surrounded by residential and commercial blocks. Trace gases (Thermo Inc. series), meteorological parameters (Vaisala Inc.), and $PM_{2.5}$ (TEOM 1430) were recorded during the observation.

The PG site (117.053ºE, 40.173ºN) is 3 km from the PG center. The site is located in the northeast of the PKU site with a distance of 70 km. The PG site also acts as a host of the AIRLESS (Effects of AIR pollution on the cardiopulmonary disease in urban and peri-

urban residents in Beijing) Project. The meteorological data is acquired from the local meteorological office. The PG village is surrounded by orchards and farmland with no main road nearby on a scale of 3 km. Coal and biomass are used for domestic heating and cooking in the nearby villages.

2.2 Instrumentation and data analysis

Two SPAMSs (Model 0515, Hexin Inc., Guangzhou, China) were deployed at both PKU and PG. A technical description of SPAMS is available in (Li et al., 2011). Briefly, a SPAMS has three functional parts: sampling, sizing, and mass spectrometry. In the sampling part, particles within a 0.1–2.0 μm size range pass efficiently through an aerodynamic lens. In the sizing unit, the aerodynamic diameter (D_{va}) is calculated using the time-of-flight of particles. The particles are then decomposed and ionized into ions one-by-one using a 266 nm laser. A bipolar time-of-flight mass spectrometer measures the ions and generates the positive and negative mass spectra of each particle. The two instruments were maintained and calibrated following the standard procedures before sampling (Chen et al., 2017).

A neural network algorithm based on adaptive resonance theory (ART-2a) was used to resolve particle types from both datasets (Song et al., 1999). The parameters used were: a vigilance factor of 0.70, a learning rate of 0.05, and 20 iterations. This procedure generated 771 and 792 particle groups. Then, the groups were combined into particle types based on similar mass spectra, temporal trends, and size distributions (Dall'osto and Harrison, 2006). During combining, relative areas of nitrate and sulfate were used to distinguish the stages of processing, assuming that more sulfate and nitrate can be measured if a particle is more

processed during its lifetime. Thus, particles with relative peak areas of sulfate and nitrate larger than 0.1 were marked with nitrate (-Nit), sulfate (-Sul), respectively, or both. Indeed, matrix effect can affect ionic intensities between different particles during single-particle mass spectrometer analysis. However, the effect can be reduced using average mass spectra of particles within the similar size distribution and chemical composition. Finally, the strategy resulted in 20 and 19 particle types at PKU and PG respectively. Among them, 17 types appeared at both sites, and each type has identical mass spectra (R^2> 0.80) between each other.

3. Results

A total of 4,499,606 and 4,063,522 particles were collected at PKU and PG sites, respectively. The size distributions peaked at 0.48 μm and 0.52 μm (Figure 1). The smaller size distribution was due to a more substantial fraction of freshly-emitted particles at PG, as described in Table 1. Seventeen particle types (R^2 > 0.80, mass spectra) were observed both at PKU and PG (Table 1). These particle types were labeled with the suffixes "_PKU" or "_PG" to indicate their locations. The term "particle category" stands for a group of particle types with variable stages of processing.

143 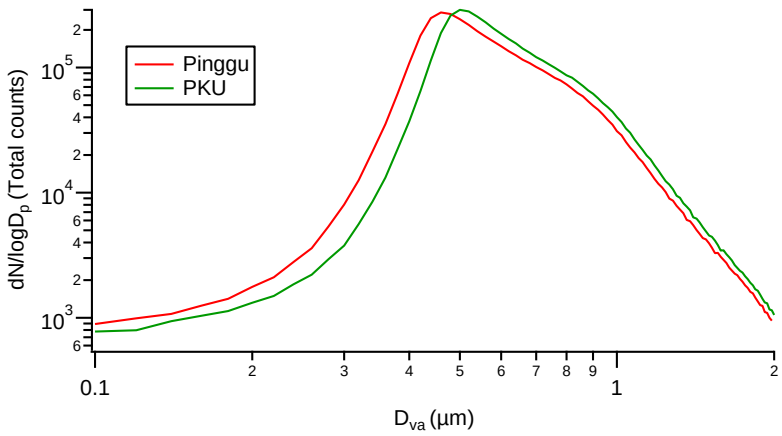

144 Figure 1. The size distribution of SPAMS particles at PKU and PG sites.

145

146 Table 1. SPAMS particle types identified at PKU and PG sites.

	PKU	PKU	PG	PG	Comments
Particle type	Number	Percentage	Number	Percentage	
EC-Nit	313574	7.0	79082	2.0	Solid fuel burning, traffic
EC-Nit-Sul	473908	10.5	140107	3.5	
EC-Sul	30365	0.7	4096	0.1	
ECOC-Nit-Sul	539533	12.0	755279	18.6	Traffic, coal burning
ECOC-Sul	572548	12.7	397367	9.8	
K-rich	322731	7.2	259287	6.4	Aged biomass burning
K-Nit	359281	8.0	334547	8.2	
K-Nit-Sul	717280	16.0	76954	1.9	
K-Sul	26301	0.6	183571	4.5	
NaK	16680	0.4	74943	1.8	Coal, peat
NaK-Nit	289259	6.4	69760	1.7	
NaK-Nit-Sul	114387	2.5	77555	1.9	
NaK-Sul	7509	0.2	16578	0.4	
OC-Nit-Sul	334870	7.4	865821	21.3	Traffic,
OC-Sul	40800	0.9	279322	6.9	coal burning
Ca-dust	19869	0.4	3035	0.1	dust
Fe-rich	137600	3.1	70920	1.8	Steel industry
ECOC-Nit	137470	3.1%			Solid fuel burning
OC-Nit	41159	0.9%			Traffic, coal burning
K-Amine-Nit-Sul	4482	0.1%			Coal burning
ECOC			239953	5.9%	Coal burning
OC			135345	3.3%	Traffic, coal burning

147

148 Note: Nit stands for nitrate, Sul for sulfate.

149 **3.1 Meteorological conditions and overview**

150 Temperature, relative humidity (RH), and wind speed at both sites during the sampling
151 period are summarized in Table 2. Their temporal trends are available in Part II. The

average temperature at PKU (urban, 5.7±2.3 °C) was higher than at PG (rural, 3.1±2.2 °C). Correspondingly, relative humidity was higher at PG (67±32%) than at PKU (49±30%). The wind was stronger at PKU (2.5± 1.8 ms^{-1}) than at PG (1.7± 0.9 ms^{-1}). As shown in Figure 2, at PKU, wind speed peaked at noon (local time, UTC+8), while at PG, wind speed reached its maxima at 15:00. Various wind speeds determined the different dispersion patterns of pollutants near the surface. It should be noticed that wind speed up to 2 ms^{-1} representing a scale of 172 km in diurnal transport. Therefore, at PKU, the wind could bring the pollutants from Hebei province under stagnant air conditions.

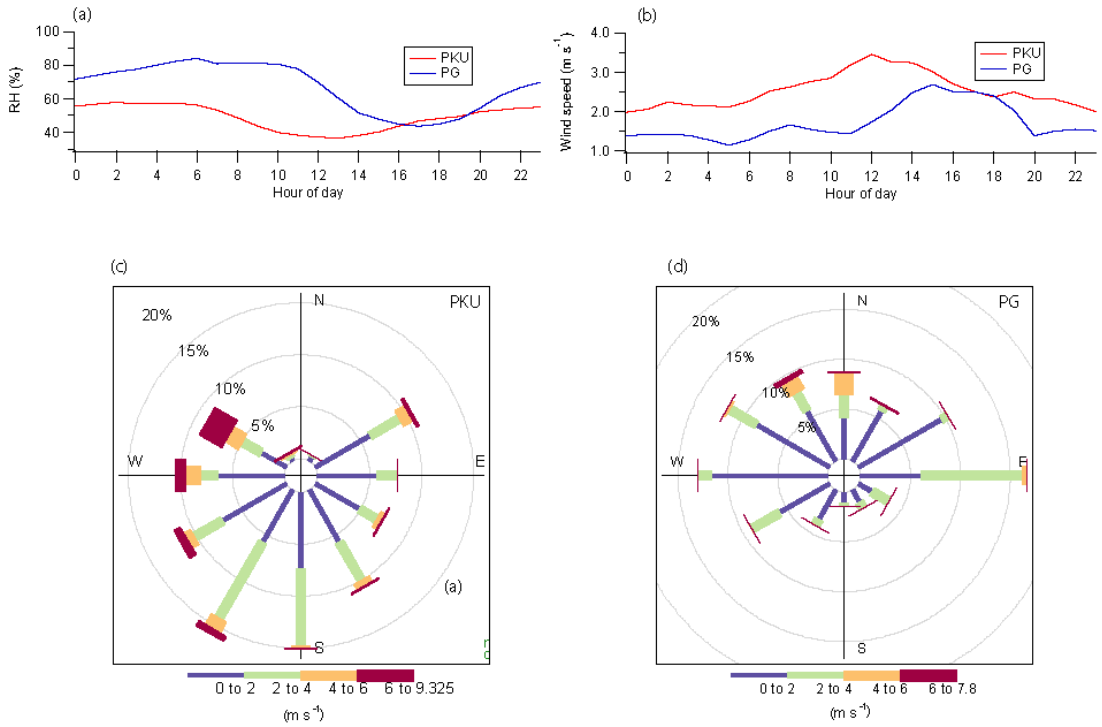

Figure 2. Diurnal plots of (a) RH and (b) wind speed, and rose plots of wind at (c)PKU and (d) PG.

Table 2. Meteorological parameters at PKU and PG during the campaign.

	PKU	PG
Temperature (°C)	5.7±2.3	3.1±2.2
RH (%)	49±30	67±32
Wind speed (ms^{-1})	2.5± 1.8	1.7± 0.9

3.2 Common particle categories at both PKU and PG

3.2.1 Elemental carbon (EC)

As shown in Figure 3a, the elemental carbon (EC) particle category was represented by ions peaking at *m*/*z* 12, 24, 36, 48, and 60 in positive mass spectra (Sodeman et al., 2005; Toner et al., 2008). EC is emitted from solid fuel combustion, traffic (Sodeman et al., 2005; Toner et al., 2008), and industrial activities (Healy et al., 2012; Liu et al., 2019a). Due to the various ionic intensities of nitrate (*m/z* -46 and -62) and sulfate (*m*/*z* -80 and -97), the EC category has four types including EC-Nitrate (EC-Nit), EC-Sulfate (EC-Sul), and EC-Nit-Sul. Besides, the EC category was more abundant after the heating began rather than before (Part II), indicating that coal burning was one of the primary sources.

EC-Nit_PKU and EC-Nit_PG accounted for 7.0% and 2.0% in PKU and PG datasets, respectively. In the diurnal profiles of EC-Nit_PKU, there was an apparent early morning peak at 5:00 (UTC+8, local time), along with an evening peak (22:00). There was also an early morning NO_x peak in the urban area of Beijing, providing sufficient precursors for secondary nitrate (Shi et al., 2019). Wang et al. (2018) validated the role of N_2O_5 uptake on the nitrate formation in PM. Therefore, the early morning peak of EC-Nit_PKU occurred due to the uptake of nitrate on the freshly emitted EC in the early morning (Sun

et al., 2014a). The evening peak could be due to the low temperature after the heating supply started (Liu et al., 2019a). Diurnally, EC-Nit_PG exhibited an early morning peak (5:00) but no evening peak and mainly came from the southeast.

EC-Nit-Sul was more abundant at the rural site (18.6%) than the urban site (11.6%). EC-Nit-Sul_PKU (10.5%) had early morning (04:00), morning (7:00), and afternoon peaks (around 16:00), while EC-Nit-Sul_PG (3.5%) had early morning (04:00), noon, and afternoon peaks (17:00, Figure 3a). However, they showed relatively small diurnal variations. For example, EC-Nit-Sul_PKU varied between 800 h^{-1} and 1,000 count h^{-1}, and EC-Nit-Sul_PG shifted between 200 count h^{-1} and 250 count h^{-1}. Thus, the EC-Nit-Sul at both sites was most likely acting as background and regional particles (Dall'Osto et al., 2016). Additionally, EC-Nit-Sul_PKU mainly came from the surrounding area in the city pollutant plume, while EC-Nit-Sul_PG mainly came from the southeast (Figure 3c).

EC-Sul was a minor type at both sites, accounting for 0.7% at PKU and 0.1% at PG. EC-Sul was pronounced in the afternoon when the wind was strong at both sites. It was unlikely for either EC-Sul_PKU or EC-Sul_PG to be local because their concentrations were associated with high wind speed, as shown in Figure 3c. More specifically, EC-Sul_PKU came from the southeast and northeast of Hebei Province when the wind speed exceeded 6 m s^{-1}. EC-Sul_PG could come from the west when the wind speed exceeded 2 m s^{-1} and the east when the wind speed exceeded 3 m s^{-1}, as coal-using industries are located in both directions. Also, at both sites, the concentrations of SO_2 were elevated in the afternoon due to transport, providing sufficient precursors for the formation of sulfate (Shi et al., 2019).

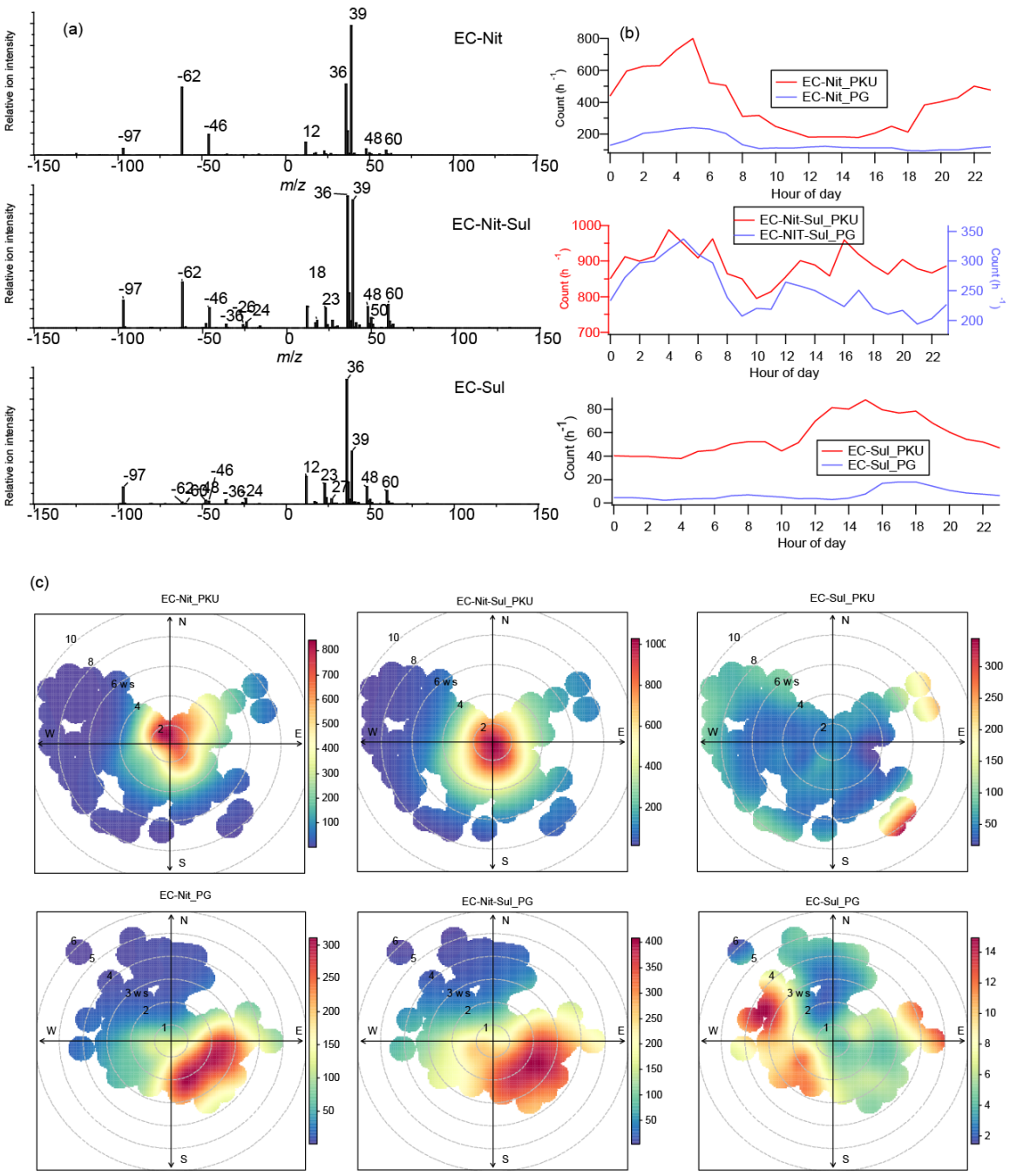

Figure 3. (a) average mass spectra of EC-Nit, EC-Nit-Sul, and EC-Sul at both sites; (b) diurnal patterns of EC-Nit, EC-Nit-Sul, and EC-Sul at both sites; (c) polar plots of EC-Nit, EC-Nit-Sul, and EC-Sul; the grey circles indicate wind speed (m s^{-1}).

3.2.2 Organic carbon (OC) category

The positive mass spectra of both OC-Nit and OC-Nit-Sul contained complicated organic ions such as $C_2H_3^+$ (*m*/*z* 27), C_3H^+ (*m*/*z* 37), $C_3H_7^+$/$C_2H_3O^+$/ $CHNO^+$ (*m*/*z* 43), $C_4H_2^+$ (*m*/*z* 50), aromatic hydrocarbons ($C_4H_3^+$, $C_5H_3^+$, and $C_6H_5^+$), and diethylamine ($(C_2H_5)_2NH_2^+$, *m*/*z* 74), $(C_2H_5)_2NCH_2^+$ (*m*/*z* 86)). The negative mass spectra contained CN^- (*m*/*z* –26), Cl^- (*m*/*z* –35 and 37), CNO^- (*m*/*z* –42), nitrate (*m*/*z* –46 and –62), and sulfate(*m*/*z* –97). The presence of CN^- and CNO^- suggests the existence of organonitrogen species (Day et al., 2010). Peak intensities of organic fragments are relatively high in the OC-Sul particles, indicating that it was relatively fresh, while OC-Nit-Sul was more processed (Zhai et al., 2015; Peng et al., 2020a). The positive mass spectrum had similar ions of Coal Combustion OA (CCOA) with significant signals of PAHs in AMS studies (Sun et al., 2013). OC-Sul showed different spatial distributions with 0.9% at PKU and 6.9% at PG.

OC-Sul_PG had morning (8:00) and afternoon (16:00) peaks, while the diurnal profile of OC-Sul_PKU showed a trend with an early morning (3:00), morning (10:00), and afternoon peaks (16:00). The diurnal trends OC-Sul at both PKU and PG were consistent with the heating pattern depending on the variation of local temperature. Moreover, OC-Sul_PG increased after the heating supply began. Polar plots suggest that OC-Sul_PKU came from surrounding southwest areas via transport, while OC-Sul_PG came from villages to the east and west (Figure 4). These results suggest that OC-Sul_PG was emitted from coal burning for residential heating in nearby areas.

OC-Nit-Sul accounted for 7.4 % and 21.3 % of all detected particles at PKU and PG, respectively. OC-Nit-Sul_PKU had a diurnal peak at 7:00 in rush hours, suggesting that

OC-Nit-Sul could be formed due to the uptake of nitrate on OC-Sul. While OC-Nit-Sul_PG had a diurnal peak at 8:00 due to traffic in nearby towns. As an aged particle type, OC-Nit-Sul_PKU and OC-Nit-Sul_PG, also acting as a similar type of background types with hourly counts remained low but elevated to high levels at night. Polar plots suggest that OC-Nit-Sul_PKU mainly came from the surrounding areas, while OC-Nit-Sul_PG mainly came from the south and east, where populous villages are located (Figure 4).

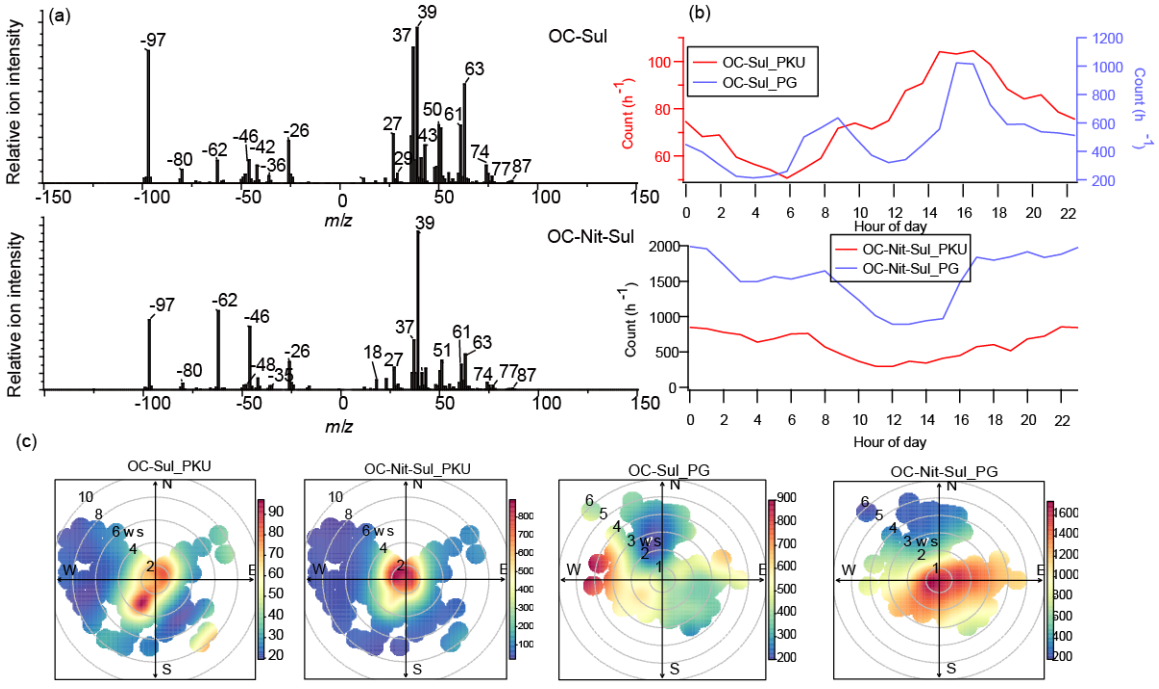

Figure 4. (a): average mass spectra of OC-Nit and OC-Nit-Sul observed at both sites; (b): diurnal patterns of the hourly count of OC-Nit and OC-Nit-Sul at both sites; (c): polar plots of OC-Sul and OC-Nit-Sul; the grey circles indicate wind speed (m s^{-1}).

3.2.3 ECOC category

As shown in Figure 5a, the ECOC category contained two major particle types: ECOC-Nit-Sul and ECOC-Sul. The positive mass spectrum of ECOC-Nit-Sul contained C_n^+ (*m/z*

12, 24, 36…), NH_4^+ (*m*/*z* 18), $C_2H_3^+$ (*m*/*z* 27), K^+ (*m*/*z* 39 and 41), $C_3H_7^+$/$C_2H_3O^+$/ $CHNO^+$ (*m*/*z* 43), $C_4H_2^+$ (*m*/*z* 50), and $[(C_2H_5)_2NH_2]^+$ (*m*/*z* 74); in the negative mass spectrum, ions such as sulfate (*m*/*z* -80 and -97), nitrate (*m*/*z* -46 and -62), C_n^-, and CN^- (*m*/*z* -26) were abundant. This mixture of EC and OC particle types was common in single particle studies. ECOC could be local, and from incomplete combustion processes (Chen et al., 2017), or regional transport, e.g., after aging (McGuire et al., 2011; Huang et al., 2013; Zhao et al., 2019). The diurnal profile of ECOC-Sul_PG showed early morning (1:00), morning (8:00), and afternoon (17:00) peaks, which is consistent with local cooking and heating patterns. Also, heating activities enhanced the fraction of ECOC-Sul_PG. ECOC-Sul_PKU did not show a clear diurnal profile, suggesting that ECOC-Sul_PKU was mainly a background type. Similarly, ECOC-Nit-Sul_PKU and ECOC-Nit-Sul_PG were also background types with less obvious diurnal variations (Dall'Osto et al., 2016). Polar plots (Figure 5c) suggested that both ECOC-Nit-Sul_PKU and ECOC-Sul_PKU had both local and regional sources. Wind speed up to 4 m s^{-1} could cause a transport with a distance of 346 km diurnally, indicating that it was possible for the particles from Hebei province to arrive at the sampling place.

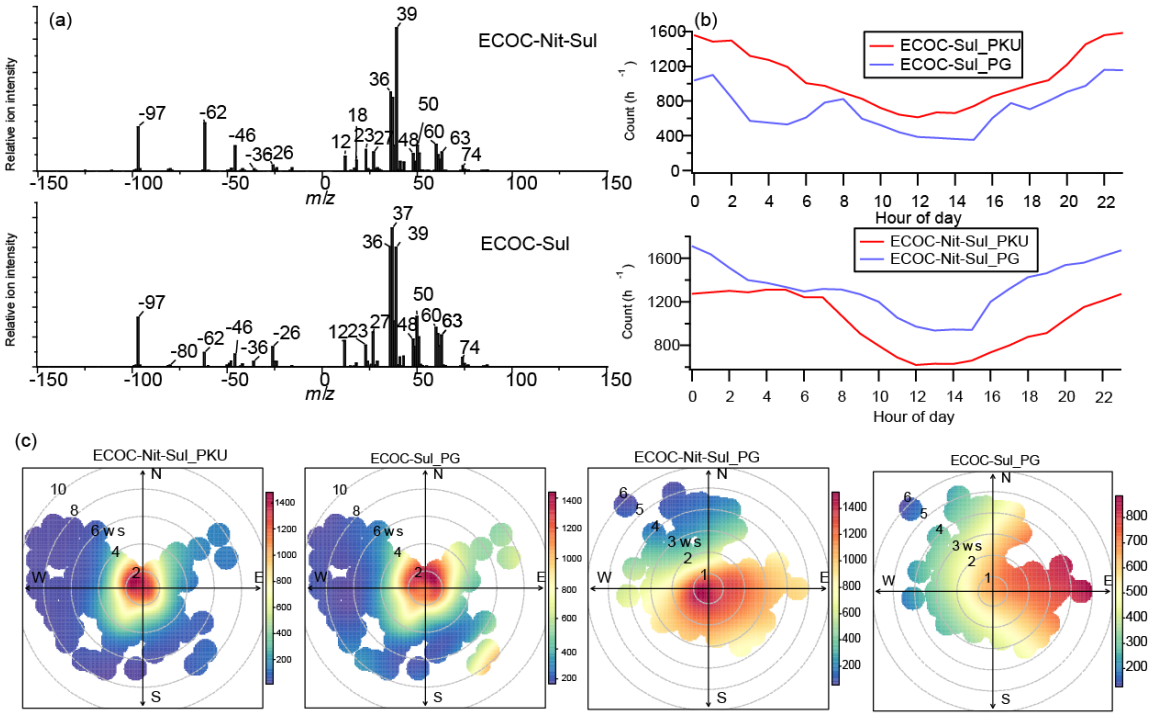

Figure 5. (a): average mass spectra of ECOC-Nit and ECOC-Nit-Sul observed at both sites; (b): diurnal patterns of the hourly count of ECOC-Sul and ECOC-Nit-Sul at both sites; (c): polar plots of ECOC-Sul and ECOC-Nit-Sul; the grey circles indicate wind speed (ms^{-1}).

3.2.4 K-rich category

Figure 6 shows a series of potassium-rich (K) particle types. K-rich contained Na^+ (*m/z* 23), $C_2H_3^+$ (*m/z* 27), C_n^+, C_3H^+ (*m/z* 37), K^+, aromatic hydrocarbons ($C_4H_3^+$, $C_5H_3^+$, and $C_6H_5^+$), levoglucosan (*m/z* -45, -59, and -71), sulfate, and nitrate. According to the ionic intensities of sulfate and nitrate, the K-rich particle category had several branches such as K-rich, K-Nit, K-Sul, and K-Nit-Sul. K-rich particles are commonly found in biomass burning emissions (Silva et al., 1999; Pagels et al., 2013; Chen et al., 2017). Cl^- was unabundant in all K-rich particle types, suggesting that the K-rich particles had undergone aging during

atmospheric processing (Sullivan et al., 2007; Chen et al., 2016), but K-Nit, K-Nit-Sul, and K-Sul were more processed.

All K-rich category particles showed different atmospheric evolution process at both PKU and PG. K-rich_PKU illustrated a typical pattern that was at low levels in the daytime but high levels at nighttime (22:00). As shown in Figure 6c, at an average wind speed of 3 m s^{-1}, it took five hours for particles from a distance of 50 km to arrive at PKU. This is also the reason why BB-related particles were abundant in urban Beijing where the household BB is prohibited. The origination of K-rich_PKU was from nearby and southwest. K-rich_PG, however, showed a pattern with cooking and heating activities, peaking at 7:00 and 17:00. The peak at 7:00 was due to the local emissions; the 17:00 could be transported from a distance of 50 km at a wind speed of 3 m s^{-1} from the east and west.

The secondary process contributed to the early morning peak (5:00) of K-Nit_PKU due to the nighttime formation of nitrate via hydrolysis of N_2O_5 in the NO_x-rich urban areas (Wang et al., 2017). In the day time, after the rush hours, the number concentration of K-Nit_PKU increased again via the uptake of nitrate due to day time photoactivity. K-Nit_PKU mainly originated from the local and southerly areas (Figure 6c). Besides the early morning peak, K-Nit_PG showed cooking and heating patterns that they were abundant when the temperature was low in the early morning and afternoon. K-Nit_PG had wide originated from both local and region via long-range transport.

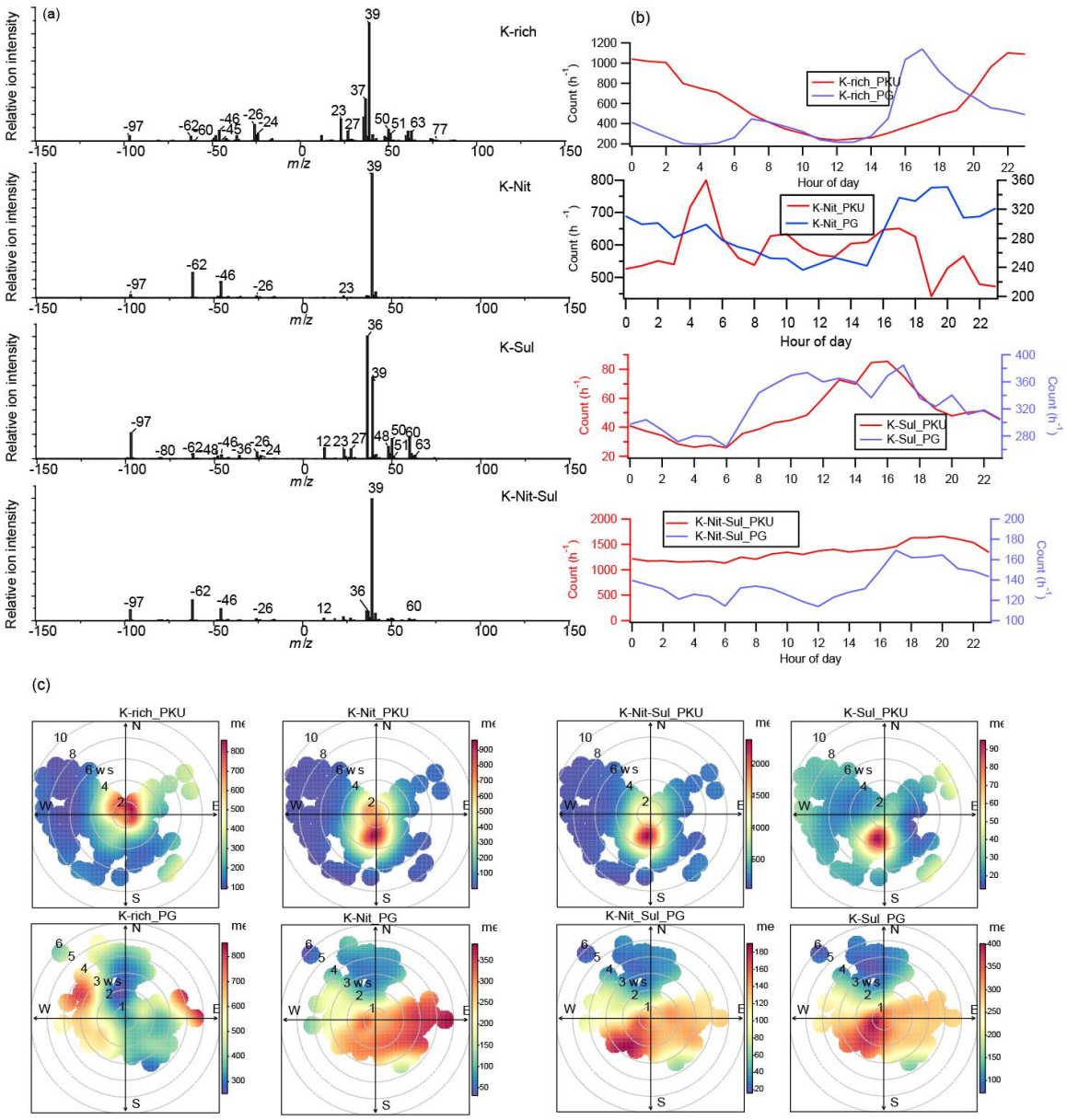

Figure 6. (a): average mass spectra of BB, K-Nit, K-Sul, and K-Nit-Sul observed at both sites; (b): diurnal patterns of the hourly count of K-rich, K-Nit, K-Sul, and K-Nit-Sul at both sites; (c): polar plots of BB, K-Nit, K-Sul, and K-Nit-Sul; the grey circles indicate wind speed (m s^{-1}).

3.2.5 Metal category

Two metal-rich particles types were identified, namely Fe-rich and Ca-rich. Fe-rich contained iron (*m*/*z* 56 and 54), K^+, Na^+, NH_4^+, Cl^- (*m*/*z* -35 and -37), sulfate, and nitrate. Ca-rich was composed of Ca^+ (*m*/*z* 40), CaO (*m*/*z* 56), K^-, Na^+, Cl^-, sulfate, and nitrate. As shown in Figure 6b, Ca-rich_PKU (0.4%) and Ca-rich_PG (0.1%) were likely of regional origin with no distinct diurnal variations. Since SiO_2^- or SiO_3^- (*m*/*z* -60 and -76) were not abundant in the Ca-rich particles, they are not likely to come from dust (Silva et al., 2000). According to its weak peaks during the rush hour at PKU, a possible source of the Ca-rich particles was from road dust re-suspension. Such rush hour peaks were not observed at PG.

Fe-rich_PKU (3.1%) and Fe-rich_PG (1.8%) had similar diurnal profiles that arose in the early morning when heavy-duty vehicles were allowed to enter the 5-ring expressway. The peak occurred earlier at PG (4:00) than (5:00) because these vehicles got close to PG earlier than to PKU. The daytime peak occurred in the afternoon at both PKU and PG when wind speed was high. Therefore, there were also multiple sources for Fe-rich particles, including re-suspended dust particles from traffic and fly ash from the steel industry. In Beijing, daytime Fe-rich particles were reported and assigned to long-range transport and industrial sources from Heibei Province (Figure 7c) (Li et al., 2014). The steel industry moved out of Beijing more than a decade ago (Liu et al., 2016b). Currently, most of these steel industries were located in the Heibei Province.

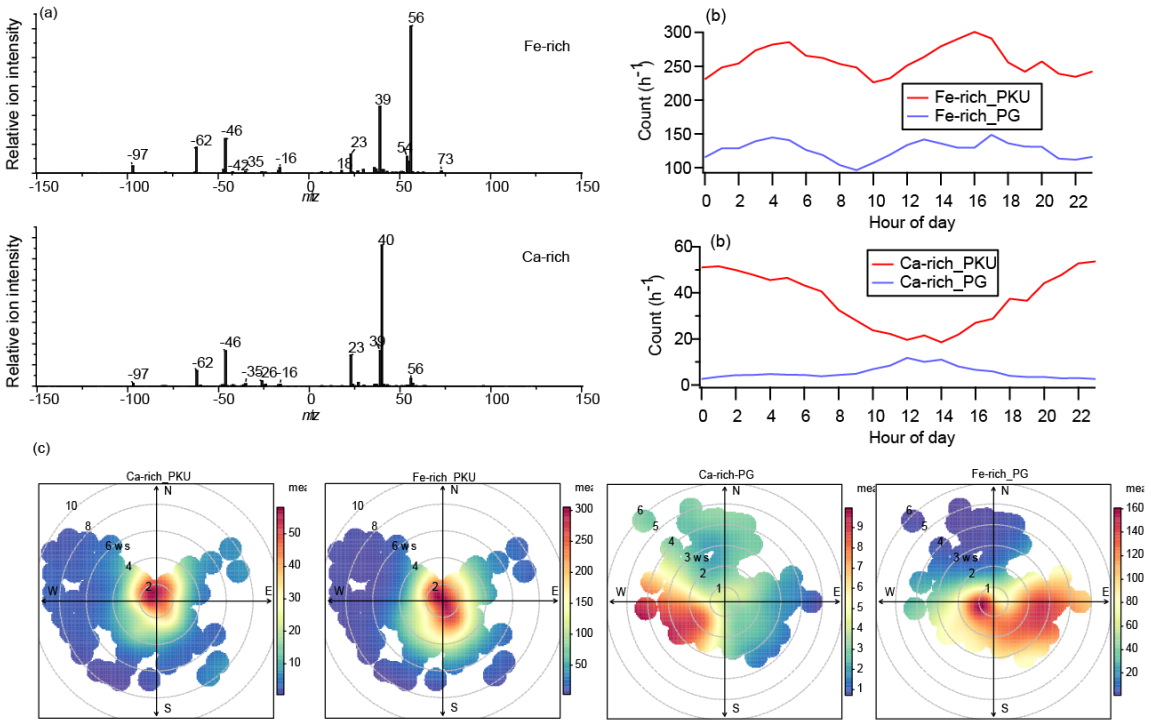

315

316 Figure 7. (a): average mass spectra of Fe-rich and Ca-rich observed at both sites; (b):
317 diurnal patterns of the hourly count of Fe-rich and Ca-rich at both sites; (c): polar plots of
318 Fe-rich and Ca-rich; the grey circles indicate wind speed (ms^{-1}).

319 **3.2.6 NaK category**

320 As shown in Figure 8, mass spectra of NaK category contained Na^+, K^+, C_n^+, C_n^-, nitrate,
321 and PO_3^- (*m*/*z* -79). The aged NaK particles contained strong signals of nitrate (NaK-Nit),
322 sulfate (NaK-Sul), or both (NaK-Nit-Sul). In general, the NaK category contained stronger
323 signals of Na^+ than the EC and K-rich categories. The NaK category may also come from
324 incomplete solid fuel combustion processes such as coal, peat, or wood (Chen et al., 2017;
325 Healy et al., 2010; Xu et al., 2017). NaK category was more abundant at PKU (9.5%) than
326 PG (5.8%), suggesting a stronger contribution of emission from coal boilers (Xu et al.,

2017; Xu et al., 2018). Additionally, after heating began, the fraction of NaK-Nit_PG and NaK-Sul-Nit_PG increased by 1.2 times (see Part II).

NaK_PKU showed no distinct diurnal variations, suggesting that it was a regional particle type arriving at the PKU site via transport, while NaK_PG showed an apparent diurnal variation consistent with cooking and heating pattern. Polar plots also suggest that they are from the east and the west. NaK-Nit, with a considerable uptake of nitrate, was more abundant at PKU (6.4%) than PG (1.7%). Both NaK-Nit_PKU and NaK-Nit _PG increased in the afternoon when photochemical activities were most active (Figure 8c). Both of them may be from regional transport (Figures 8b and 8c).

NaK-Sul was a minor particle type at both PG and PKU, accounting for 0.2% and 0.4%, respectively. The diurnal profile of NaK-Sul_PG was also following the local cooking and heating pattern, while NaK-Sul_PKU showed a typical transport pattern that became abundant in the afternoon as the southwestern wind speed increased. As a heavily aged particle type, NaK-Nit-Sul was transported to both PKU and PG from the southwest. In short, NaK-related particle types mainly came from the solid fuel burning process, e.g., coal. Due to its different origins, it showed different levels of processing at PKU and PG, respectively.

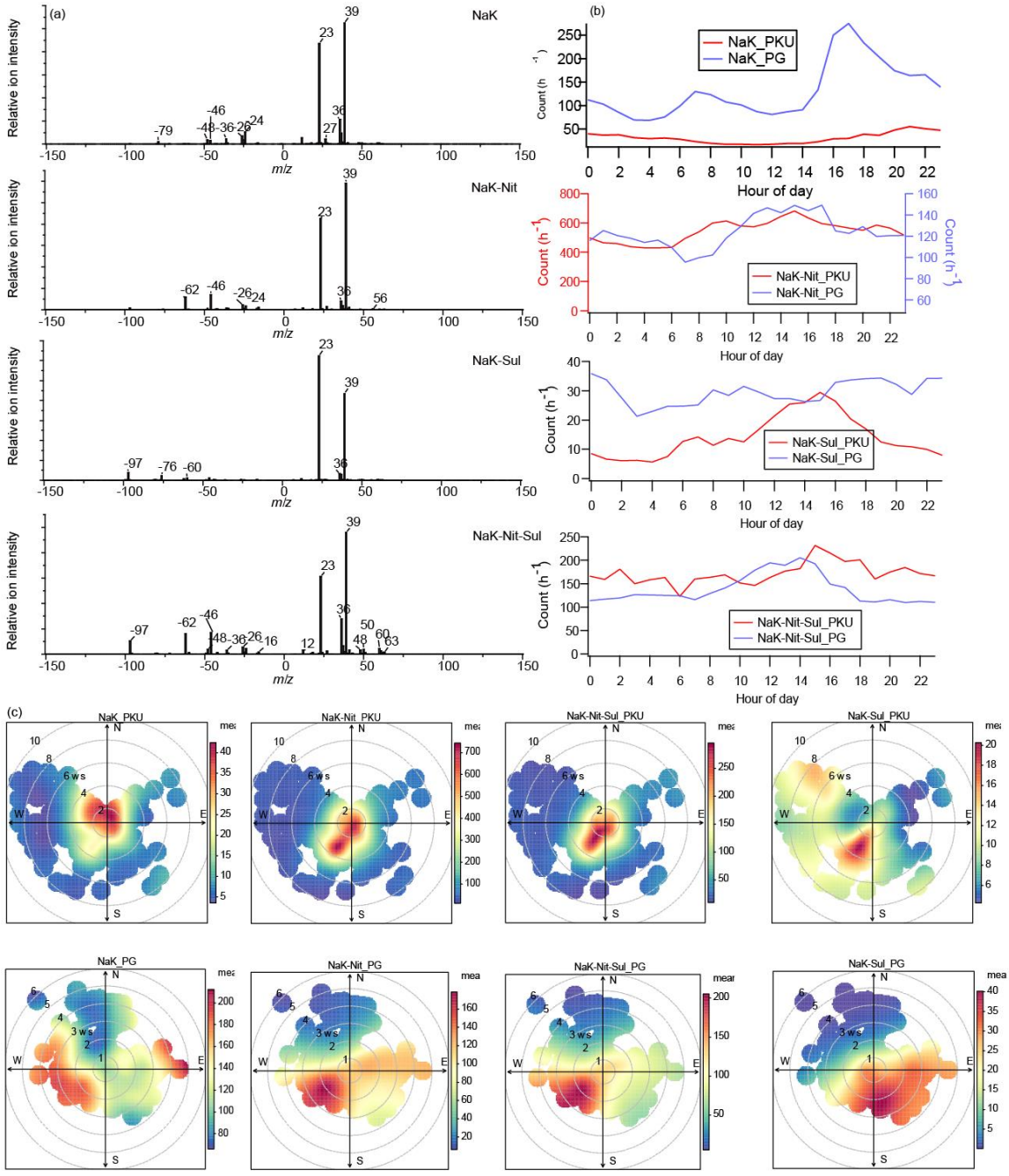

Figure 8. (a): average mass spectra of NaK, NaK-Nit, NaK-Nit-Sul, and NaK-Sul observed at both sites; (b): diurnal patterns of the hourly count of NaK, NaK-Nit, NaK-Nit-Sul, and NaK-Sul at both sites; (c): polar plots of NaK, NaK-Nit, NaK-Nit-Sul, and NaK-Sul; the grey circles indicate wind speed (m s^{-1}).

3.3 Unique Particle types at the PKU site

OC-Nit_PKU (0.9%) and ECOC-Nit_PKU (3.1%) with strong ion intensities of nitrate were observed at the PKU site. OC-Nit_PKU and ECOC-Nit_PKU showed a peak at night than at daytime, similar to the diurnal profiles of OC-Nit-Sul_PKU and ECOC-Nit-Sul_PKU. Such nitrate-rich particle types could have come from the uptake of nitrate in OC and ECOC(Qin et al., 2012; Chen et al., 2016). Polar plots suggest that both types were formed locally when the wind speed was lower than 4 ms^{-1}. The NO_x-rich environment in urban Beijing provides a favorable condition for nitrate formation at night (Wang et al., 2016; Shi et al., 2019).

A minor amount (0.10%) of amine-containing particles was observed at the PKU site, and trimethylamine ion fragments (*m*/*z* 58 and 59) were influential in the mass spectrum of K-amine-Nit-Sul_PKU (Figure 9a). The diurnal profile of K-amine-Nit-Sul_PKU showed an afternoon peak, indicating a regional source (Figure 9c). K-amine-Nit-Sul_PKU was transported to the site from nearby locations. The amines may come from animal husbandry, BB, traffic, or vegetation (Chen et al., 2019b). Amines were ubiquitous in the atmospheric environment, playing essential roles in new particle formation and growth, as well as fog and cloud processing (Ge et al., 2011; Chen et al., 2019b).

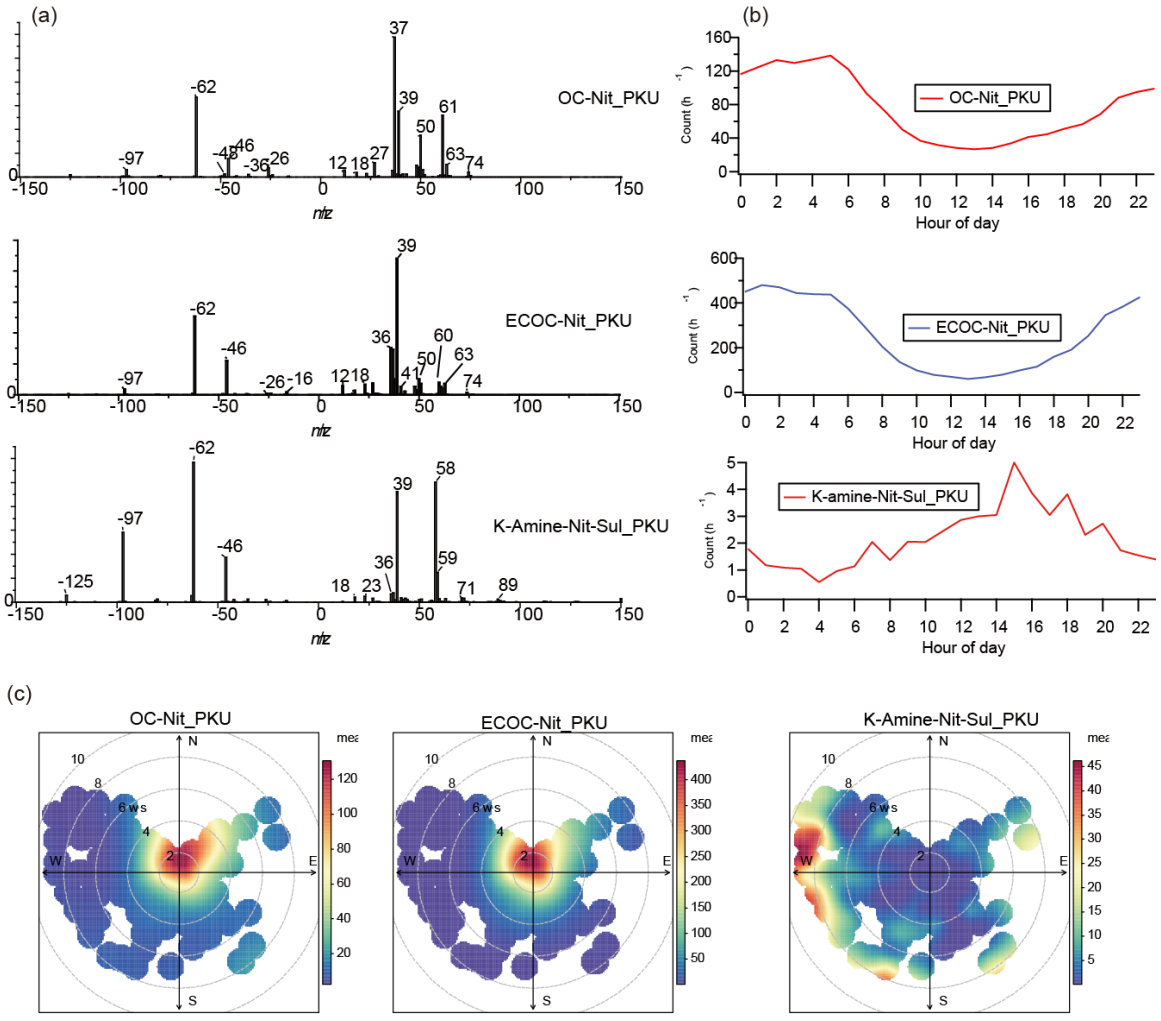

366

367 Figure 9. (a): average mass spectra of OC-Nit_PKU, ECOC-Nit_PKU, and K-amine-Nit-
368 Sul_PKU observed at the PKU site; (b): diurnal patterns of the hourly count of OC-
369 Nit_PKU, ECOC-Nit_PKU, and K-amine-Nit-Sul_PKU at the PKU site; (c): polar plots of
370 OC-Nit_PKU, ECOC-Nit_PKU, and K-amine-Nit-Sul_PKU, and the grey circles indicate
371 wind speed (m s^{-1}).

372 **3.4 Unique Particle types at the PG site**

373 OC_PG (5.9%) and ECOC_PG (3.3%) were only observed at the rural site PG (Figure 10).
374 The major components of these two types were consistent with the OC and ECOC

categories, respectively, but with limited uptake of sulfate and nitrate, suggesting that they were possibly freshly emitted particles(Peng et al., 2020b). Their diurnal profiles are consistent with cooking and heating patterns which peaked at 07:00 in the morning and 17:00. Polar plots suggest that OC_PG mainly came from nearby and other remote areas in all directions except the north. ECOC mainly came from the east of the PG site. These results supported the assumption that the two types were mainly from local emission sources. Also, the emission of OC_PG and ECOC_PG is popular in the region.

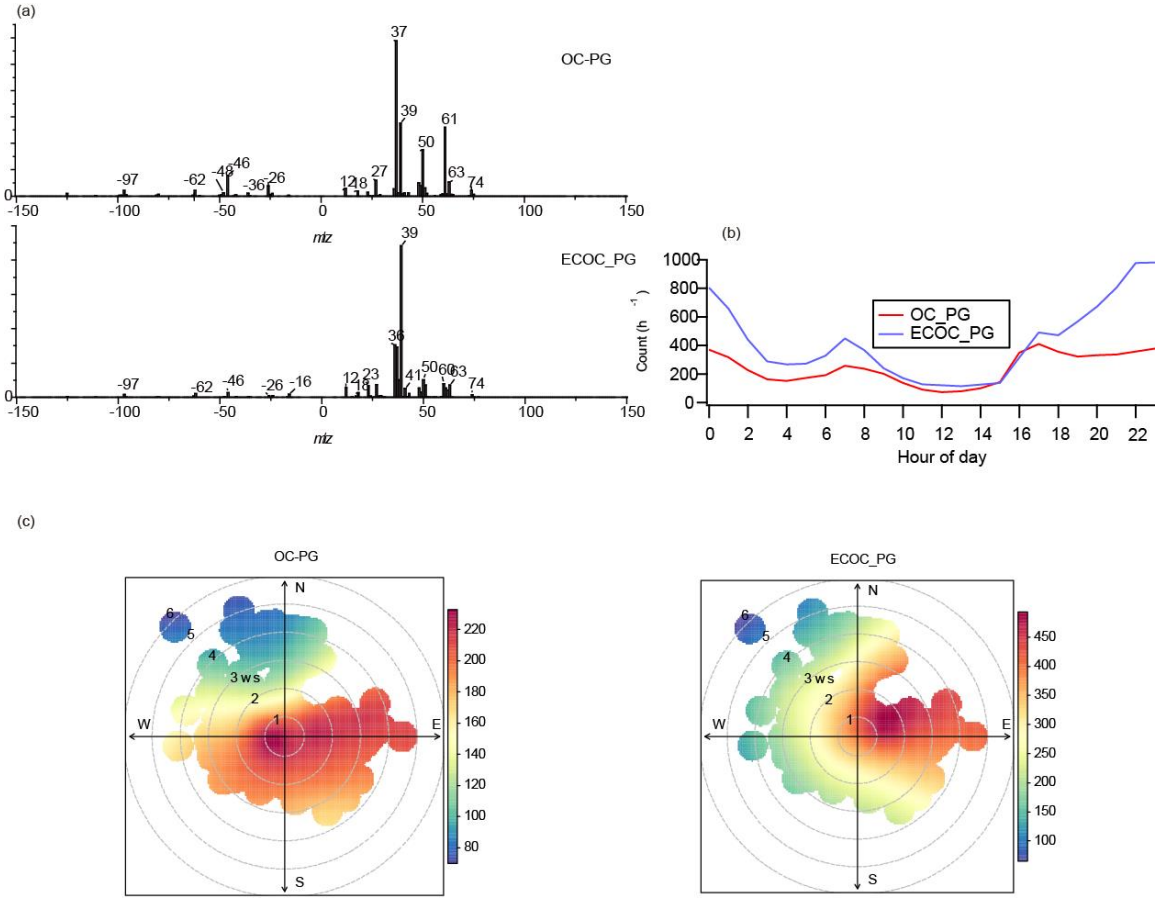

Figure 10. (a) Average mass spectra of OC_PG and ECOC_PG, (c) diurnal plots of OC_PG and ECOC_PG, and (c) polar plots of OC_PG and ECOC_PG. All these particle types appeared at the PG site.

4. Discussion

Multiple source apportionment models have been used in Beijing to quantify the sources of particles (Sun et al., 2014a; Xu et al., 2015; Zhai et al., 2016). Biomass burning, coal combustion, traffic, and dust are the key sources of PM (Sun et al., 2014a; Liu et al., 2018; Huang et al., 2014). Multiple studies confirmed that biomass burning is an essential source of PM in urban Beijing (Gao et al., 2014; Huang et al., 2014; Sun et al., 2014a; Zheng et al., 2017). In this study, biomass burning, and other solid fuel burning were identified as crucial sources of PM in not only urban but also rural areas of Beijing. We observed that BB-related particles (K-rich category) were more abundant at PG than at PKU. In particular, we found fresh-emitted K-containing particles at the Pinggu site, confirmed the importance of local emissions to PM. Furthermore, K-containing particles in the urban area were more aged, suggested that they are aged and mostly from the surrounding areas. The result is consistent with the results from (Liu et al., 2019b) based on a combined receptor and footprint models. Nevertheless, household emissions in the BHT region caused 32% and 15% of primary $PM_{2.5}$ and SO_2. These studies have proved the importance of household emission from BB in the BHT area (Liu et al., 2016a). Especially at the PG site, the ambient PM was mainly controlled by long-range transport and household emissions from cooking and heating.

Due to the nature of SPAMS, the chemical composition of PM cannot be precisely quantified. However, single particle aerosol mass spectrometers have advantages in studying the chemical composition, mixing state, source, and process of particles (Pratt and Prather, 2012). Mass-based technologies can not differentiate the origin of the bulk of nitrate, whether it is transported or formed locally. Indeed, single particle types in urban

409 Beijing have been reported in previous studies (Li et al., 2014; Liu et al., 2016b), and the
410 major types are consistent with this study. However, in this study, we adopted a cluster
411 strategy considering the relative ion peak area of sulfate and nitrate as indicators of particle
412 processing. Therefore, more details could be extracted from both two simultaneous datasets.
413 We confirmed that the source, origination, and processes were different for these particles
414 in the urban and rural areas. For example, the seriously processed particles, such as K-Nit-
415 Sul, OC-Nit-Sul, and NaK-Nit-Sul, acted with no distinct diurnal patterns as background
416 or regional sources (Xie et al., 2019). The processed particles, such as OC-Nit, ECOC-Nit,
417 and NaK-Nit, were affected by emissions and secondary formations.

418 The emission and transport patterns were different in the urban and rural areas, resulting in
419 different characteristics of PM. For example, EC particles were a key component at PKU
420 (18.2% in total), but a minor particle type at PG (5.6%). Meanwhile, in the urban area of
421 Beijing, direct emission of K-rich particles should be limited due to strict control measures;
422 thus, the K-Nit-Sul particles are mainly from long-range transport. Transported particles
423 were aged and commonly coated a thick layer of nitrate and sulfate, but the local particles
424 were affected by both emission and the near-surface aging process. For example, at PKU,
425 the primary emission sources were traffic and central heating supply, causing a NO_x-rich
426 region in which freshly-emitted particle types could undergo processing due to the uptake
427 of nitrate (Wang et al., 2016). In the nearby villages of PG, domestic heating and cooking
428 were the major contributors of primary particles when the temperature was low in the
429 morning and afternoon, resulting in the emission of multiple primary particle types such as
430 OC_PG and ECOC_PG. In short, the characteristics of PM in urban and rural areas of

Beijing were affected by local emissions and interacted with each other due to regional transport.

SO_2 was strictly controlled in Beijing. However, the emission of SO_2 is still significant in the nearby Hebei and Shandong provinces (Shi et al. 2019). The different control measures produced a low concentration area of SO_2 around Beijing. Sulfate-rich particle types such as EC-Sul, OC-Sul, K-Sul, and NaK-Sul usually arrived at the PKU site when the wind speed was high (> 3m s^{-1}). The wind directions, along with the transport of sulfate-rich particles, were east, southwest and south. In these directions, sulfate was either primarily emitted from coal burning for residential heating, power generation and industry, or secondary uptake on pre-existing particles (Zhang et al., 2015; Peng et al., 2020a). Likewise, a portion of sulfate-rich particle arrived at the PG site when the wind speed was high. However, locally formed sulfate was also pronounced, especially for ECOC-Sul, K-Sul, and NaK-Sul. As discussed in Section 3, ECOC-Sul and NaK-Sul were mainly from coal burning for residential heating, and K-Sul was formed due to the uptake of secondary sulfate. Conclusively, the particulate characterization in rural areas around Beijing is significantly influenced by residential coal burning.

Secondary nitrate formation is still a critical issue in Beijing. The daytime arising of nitrate has been reported in studies (Sun et al., 2013), and we also found a similar predominant of nitrogen-containing particles in this study. Recent studies have reported the early morning peaks of nitrate using a soot particle aerosol mass spectrometer (SP-AMS) (Wang et al., 2019), which is consistent with our results. Interestingly, the early morning peak was only observed for several particle types at both sites, including EC-Nit_PKU, K-Nit_PKU, EC-Nit-Sul-PG, and EC-Nit_PG. This result is not surprising because PG is also a NO_2-rich

region (Shi et al., 2019). The increasing contribution of nitrate-containing particles suggests the role of night chemistry in nitrate uptake on particles. Wang et al. (2017) revealed the importance of night N_2O_5 chemistry on nocturnal nitrate formation in the urban area of Beijing. The heterogeneous hydrolysis of N_2O_5 was most favorable when NO was at a low level. Moreover, the polar plots suggested a small role of long-range transport to the nitrate in individual particles. The contribution of local traffic was insignificant at the PG site as it was far from highways and major roads, the nighttime formation of nitrate appeared to be important in PG as well.

5. Conclusion

Two SPAMSs were simultaneously deployed at urban and rural sites in Beijing in order to characterize PM during wintertime. The results at both sites indicate that they shared 17 types of common clusters, most of which belonged to particle categories such as EC, OC, ECOC, BB, and NaK. The origins and sources of these particle types at both sampling sites are also comprehensively analyzed. Most of the processed PM, including EC-Nit-Sul_PKU, ECOC-Nit-Sul_PKU, and NaK-Nit-Sul_PKU, were aged locally in a NO_x-rich environment, while EC-Nit-Sul_PG, ECOC-Nit-Sul_PG, NaK-Nit-Sul_PG, and OC-Nit-Sul_PG were regional. Domestic heating in the rural area was found to be an important source of PM, and such heating activities typically caused three diurnal peaks in the early morning, morning, and afternoon (after sunset). Moreover, the early morning peak of nitrate was observed at both sites, suggesting the contribution of the heterogeneous hydrolysis of N_2O_5 in the dark during the winter. The insights gained in this study can provide useful references for understanding the relationship between regional transport and

local aging in both urban and rural areas in Beijing. In Part II, we focus on haze events observed at both sites and attempt to determine the effects of heating activities and possible regional transport between PKU and PG.

Data availability. All data described in this study are available upon request from the corresponding authors.

Author contributions. FY, MZ, TZ, QZ, and KH designed the experiments; YC, JC, ZW, MT, CP, and HY carried them out; XYang, XYao, YL, GS, and ZS analyzed the experimental data; YC prepared the manuscript with contributions from all coauthors.

Competing interests. The authors declare that they have no conflict of interest.

Acknowledgments. We are grateful for financial support from the National Natural Science Foundation of China (Grant No. 4170030287 and 81571130100). ZS acknowledges funding from NERC (NE/N007190/1 and NE/R005281/1).

References

Bi, X., Zhang, G., Li, L., Wang, X., Li, M., Sheng, G., Fu, J., and Zhou, Z.: Mixing state of biomass burning particles by single particle aerosol mass spectrometer in the urban area of PRD, China, Atmos. Environ., 45, 3447-3453, 10.1016/j.atmosenv.2011.03.034, 2011.

Cai, J., Wang, J., Zhang, Y., Tian, H., Zhu, C., Gross, D. S., Hu, M., Hao, J., He, K., and Wang, S.: Source apportionment of Pb-containing particles in Beijing during January 2013, Environ Pollut, 226, 30-40, 2017.

Chen, Y., Cao, J., Huang, R., Yang, F., Wang, Q., and Wang, Y.: Characterization, mixing state, and evolution of urban single particles in Xi'an (China) during wintertime haze days, Sci. Total Environ., 573, 937-945, 10.1016/j.scitotenv.2016.08.151, 2016.

Chen, Y., Wenger, J. C., Yang, F., Cao, J., Huang, R., Shi, G., Zhang, S., Tian, M., and Wang, H.: Source characterization of urban particles from meat smoking activities in Chongqing, China using single particle aerosol mass spectrometry, Environ. Pollut., 228, 92-101, 10.1016/j.envpol.2017.05.022, 2017.

Chen, Y., Liu, H., Huang, R. J., Yang, F., Tian, M., Yao, X., Shen, Z., Yan, L., and Cao, J.: Atmospheric Processing of Loess Particles in a Polluted Urban Area of Northwestern China, J. Geophys. Res. Atmos., 124, 7919-7929, 10.1029/2018jd029956, 2019a.

Chen, Y., Tian, M., Huang, R.-J., Shi, G., Wang, H., Peng, C., Cao, J., Wang, Q., Zhang, S., Guo, D., Zhang, L., and Yang, F.: Characterization of urban amine-containing particles in southwestern China: seasonal variation, source, and processing, Atmos. Chem. Phys., 19, 3245-3255, 10.5194/acp-19-3245-2019, 2019b.

Cheng, Y., Zheng, G., Wei, C., Mu, Q., Zheng, B., Wang, Z., Gao, M., Zhang, Q., He, K., and Carmichael, G.: Reactive nitrogen chemistry in aerosol water as a source of sulfate during haze events in China, Science Advances, 2, e1601530, 2016.

Dall'osto, M., and Harrison, R.: Chemical characterisation of single airborne particles in Athens (Greece) by ATOFMS, Atmos. Environ., 40, 7614-7631, 10.1016/j.atmosenv.2006.06.053, 2006.

Dall'Osto, M., Beddows, D., McGillicuddy, E. J., Esser-Gietl, J. K., Harrison, R. M., and Wenger, J. C.: On the simultaneous deployment of two single-particle mass spectrometers

518 at an urban background and a roadside site during SAPUSS, Atmos. Chem. Phys., 16,
519 9693-9710, 2016.

520 Day, D. A., Liu, S., Russell, L. M., and Ziemann, P. J.: Organonitrate group concentrations
521 in submicron particles with high nitrate and organic fractions in coastal southern California,
522 Atmos Environ, 44, 1970-1979, 10.1016/j.atmosenv.2010.02.045, 2010.

523 Du, W., Zhao, J., Wang, Y., Zhang, Y., Wang, Q., Xu, W., Chen, C., Han, T., Zhang, F.,
524 Li, Z., Fu, P., Li, J., Wang, Z., and Sun, Y.: Simultaneous measurements of particle number
525 size distributions at ground level and 260 m on a meteorological tower in urban Beijing,
526 China, Atmos. Chem. Phys., 17, 6797-6811, 10.5194/acp-17-6797-2017, 2017.

527 Gao, J., Zhang, Y., Zhang, M., Zhang, J., Wang, S., Tao, J., Wang, H., Luo, D., Chai, F.,
528 and Ren, C.: Photochemical properties and source of pollutants during continuous pollution
529 episodes in Beijing, October, 2011, J Environ Sci-China, 26, 44-53, 10.1016/s1001-
530 0742(13)60379-4, 2014.

531 Gard, E., Mayer, J. E., Morrical, B. D., Dienes, T., Fergenson, D. P., and Prather, K. A.:
532 Real-time analysis of individual atmospheric aerosol particles: Design and performance of
533 a portable ATOFMS, Anal. Chem., 69, 4083-4091, 1997.

534 Ge, X., Wexler, A. S., and Clegg, S. L.: Atmospheric amines – Part I. A review, Atmos.
535 Environ., 45, 524-546, 10.1016/j.atmosenv.2010.10.012, 2011.

536 Guo, S., Hu, M., Guo, Q., Zhang, X., Zheng, M., Zheng, J., Chang, C. C., Schauer, J. J.,
537 and Zhang, R.: Primary sources and secondary formation of organic aerosols in Beijing,
538 China, Environ. Sci. Technol., 46, 9846-9853, 10.1021/es2042564, 2012.

539 Guo, S., Hu, M., Zamora, M. L., Peng, J., Shang, D., Zheng, J., Du, Z., Wu, Z., Shao, M.,
540 Zeng, L., Molina, M. J., and Zhang, R.: Elucidating severe urban haze formation in China,
541 Proc. Natl. Acad. Sci. U.S.A., 111, 17373-17378, 10.1073/pnas.1419604111, 2014.

542 He, K., Yang, F., Ma, Y., Zhang, Q., Yao, X., Chan, C. K., Cadle, S., Chan, T., and Mulawa,
543 P.: The characteristics of PM2.5 in Beijing, China, Atmos. Environ., 35, 4959-4970,
544 10.1016/s1352-2310(01)00301-6, 2001.

545 Healy, R. M., Hellebust, S., Kourtchev, I., Allanic, A., amp, apos, Connor, I. P., Bell, J.
546 M., Healy, D. A., Sodeau, J. R., and Wenger, J. C.: Source apportionment of PM2.5 in
547 Cork Harbour, Ireland using a combination of single particle mass spectrometry and
548 quantitative semi-continuous measurements, Atmos. Chem. Phys., 10, 9593-9613,
549 10.5194/acp-10-9593-2010, 2010.

550 Healy, R. M., Sciare, J., Poulain, L., Kamili, K., Merkel, M., Müller, T., Wiedensohler, A.,
551 Eckhardt, S., Stohl, A., Sarda-Estève, R., McGillicuddy, E., amp, apos, Connor, I. P.,
552 Sodeau, J. R., and Wenger, J. C.: Sources and mixing state of size-resolved elemental
553 carbon particles in a European megacity: Paris, Atmos. Chem. Phys., 12, 1681-1700,
554 10.5194/acp-12-1681-2012, 2012.

555 Huang, M., Hao, L., Guo, X., Hu, C., Gu, X., Zhao, W., Wang, Z., Fang, L., and Zhang,
556 W.: Characterization of secondary organic aerosol particles using aerosol laser time-of-
557 flight mass spectrometer coupled with FCM clustering algorithm, Atmos. Environ., 64, 85-
558 94, 10.1016/j.atmosenv.2012.09.044, 2013.

559 Huang, R. J., Zhang, Y., Bozzetti, C., Ho, K. F., Cao, J. J., Han, Y., Daellenbach, K. R.,
560 Slowik, J. G., Platt, S. M., Canonaco, F., Zotter, P., Wolf, R., Pieber, S. M., Bruns, E. A.,

561 Crippa, M., Ciarelli, G., Piazzalunga, A., Schwikowski, M., Abbaszade, G., Schnelle-Kreis,
562 J., Zimmermann, R., An, Z., Szidat, S., Baltensperger, U., El Haddad, I., and Prevot, A. S.:
563 High secondary aerosol contribution to particulate pollution during haze events in China,
564 Nature, 514, 218-222, 10.1038/nature13774, 2014.

565 Huang, X.-F., He, L.-Y., Hu, M., and Zhang, Y.-H.: Annual variation of particulate organic
566 compounds in PM2.5 in the urban atmosphere of Beijing, Atmos. Environ., 40, 2449-2458,
567 10.1016/j.atmosenv.2005.12.039, 2006.

568 Huang, X. F., He, L. Y., Hu, M., Canagaratna, M. R., Sun, Y., Zhang, Q., Zhu, T., Xue, L.,
569 Zeng, L. W., Liu, X. G., Zhang, Y. H., Jayne, J. T., Ng, N. L., and Worsnop, D. R.: Highly
570 time-resolved chemical characterization of atmospheric submicron particles during 2008
571 Beijing Olympic Games using an Aerodyne High-Resolution Aerosol Mass Spectrometer,
572 Atmos. Chem. Phys., 10, 8933-8945, 10.5194/acp-10-8933-2010, 2010.

573 Li, L., Huang, Z., Dong, J., Li, M., Gao, W., Nian, H., Fu, Z., Zhang, G., Bi, X., Cheng, P.,
574 and Zhou, Z.: Real time bipolar time-of-flight mass spectrometer for analyzing single
575 aerosol particles, Int. J. Mass spectrom., 303, 118-124, 10.1016/j.ijms.2011.01.017, 2011.

576 Li, L., Li, M., Huang, Z., Gao, W., Nian, H., Fu, Z., Gao, J., Chai, F., and Zhou, Z.:
577 Ambient particle characterization by single particle aerosol mass spectrometry in an urban
578 area of Beijing, Atmos. Environ., 94, 323-331, 10.1016/j.atmosenv.2014.03.048, 2014.

579 Li, P., Yan, R., Yu, S., Wang, S., Liu, W., and Bao, H.: Reinstate regional transport of
580 PM2.5 as a major cause of severe haze in Beijing, Proc Natl Acad Sci U S A, 112, E2739-
581 2740, 10.1073/pnas.1502596112, 2015.

582 Liu, D., Joshi, R., Wang, J., Yu, C., Allan, J. D., Coe, H., Flynn, M. J., Xie, C., Lee, J.,
583 Squires, F., Kotthaus, S., Grimmond, S., Ge, X., Sun, Y., and Fu, P.: Contrasting physical
584 properties of black carbon in urban Beijing between winter and summer, Atmos. Chem.
585 Phys., 19, 6749-6769, 10.5194/acp-19-6749-2019, 2019a.

586 Liu, J., Mauzerall, D. L., Chen, Q., Zhang, Q., Song, Y., Peng, W., Klimont, Z., Qiu, X.,
587 Zhang, S., Hu, M., Lin, W., Smith, K. R., and Zhu, T.: Air pollutant emissions from
588 Chinese households: A major and underappreciated ambient pollution source, Proceedings
589 of the National Academy of Sciences, 113, 7756-7761, 10.1073/pnas.1604537113, 2016a.

590 Liu, L., Wang, Y., Du, S., Zhang, W., Hou, L., Vedal, S., Han, B., Yang, W., Chen, M.,
591 and Bai, Z.: Characteristics of atmospheric single particles during haze periods in a typical
592 urban area of Beijing: A case study in October, 2014, J Environ Sci-China, 40, 145-153,
593 10.1016/j.jes.2015.10.027, 2016b.

594 Liu, Y., Zheng, M., Yu, M., Cai, X., Du, H., Li, J., Zhou, T., Yan, C., Wang, X., Shi, Z.,
595 Harrison, R. M., Zhang, Q., and He, K.: High Time Resolution Source Apportionment of
596 PM_{2.5} in Beijing with Multiple Models, Atmospheric Chemistry
597 and Physics Discussions, 2018, 1-31, 10.5194/acp-2018-1234, 2018.

598 Liu, Y., Zheng, M., Yu, M., Cai, X., Du, H., Li, J., Zhou, T., Yan, C., Wang, X., Shi, Z.,
599 Harrison, R. M., Zhang, Q., and He, K.: High-time-resolution source apportionment of
600 PM_{2.5} in Beijing with multiple models, Atmos Chem Phys, 19,
601 6595-6609, 10.5194/acp-19-6595-2019, 2019b.

602 Ma, L., Li, M., Huang, Z., Li, L., Gao, W., Nian, H., Zou, L., Fu, Z., Gao, J., Chai, F., and
603 Zhou, Z.: Real time analysis of lead-containing atmospheric particles in Beijing during

springtime by single particle aerosol mass spectrometry, Chemosphere, 154, 454-462, 10.1016/j.chemosphere.2016.04.001, 2016.

McGuire, M. L., Jeong, C. H., Slowik, J. G., Chang, R. Y. W., Corbin, J. C., Lu, G., Mihele, C., Rehbein, P. J. G., Sills, D. M. L., Abbatt, J. P. D., Brook, J. R., and Evans, G. J.: Elucidating determinants of aerosol composition through particle-type-based receptor modeling, Atmos. Chem. Phys., 11, 8133-8155, 10.5194/acp-11-8133-2011, 2011.

Pagels, J., Dutcher, D. D., Stolzenburg, M. R., McMurry, P. H., Gälli, M. E., and Gross, D. S.: Fine-particle emissions from solid biofuel combustion studied with single-particle mass spectrometry: Identification of markers for organics, soot, and ash components, J. Geophys. Res. Atmos., 118, 859-870, 10.1029/2012jd018389, 2013.

Peng, C., Tian, M., Wang, X., Yang, F., Shi, G., Huang, R.-J., Yao, X., Wang, Q., Zhai, C., Zhang, S., Qian, R., Cao, J., and Chen, Y.: Light absorption of brown carbon in PM2.5 in the Three Gorges Reservoir region, southwestern China: Implications of biomass burning and secondary formation, Atmos. Environ., 229, 117409, 10.1016/j.atmosenv.2020.117409, 2020a.

Peng, C., Yang, F., Tian, M., Shi, G., Li, L., Huang, R. J., Yao, X., Luo, B., Zhai, C., and Chen, Y.: Brown carbon aerosol in two megacities in the Sichuan Basin of southwestern China: Light absorption properties and implications, Sci. Total Environ., 719, 137483, 10.1016/j.scitotenv.2020.137483, 2020b.

Pratt, K. A., and Prather, K. A.: Mass spectrometry of atmospheric aerosols--recent developments and applications. Part II: On-line mass spectrometry techniques, Mass Spectrom. Rev., 31, 17-48, 10.1002/mas.20330, 2012.

Qin, X., Pratt, K. A., Shields, L. G., Toner, S. M., and Prather, K. A.: Seasonal comparisons of single-particle chemical mixing state in Riverside, CA, Atmos. Environ., 59, 587-596, 10.1016/j.atmosenv.2012.05.032, 2012.

Shi, Z., Vu, T., Kotthaus, S., Harrison, R. M., Grimmond, S., Yue, S., Zhu, T., Lee, J., Han, Y., Demuzere, M., Dunmore, R. E., Ren, L., Liu, D., Wang, Y., Wild, O., Allan, J., Acton, W. J., Barlow, J., Barratt, B., Beddows, D., Bloss, W. J., Calzolai, G., Carruthers, D., Carslaw, D. C., Chan, Q., Chatzidiakou, L., Chen, Y., Crilley, L., Coe, H., Dai, T., Doherty, R., Duan, F., Fu, P., Ge, B., Ge, M., Guan, D., Hamilton, J. F., He, K., Heal, M., Heard, D., Hewitt, C. N., Hollaway, M., Hu, M., Ji, D., Jiang, X., Jones, R., Kalberer, M., Kelly, F. J., Kramer, L., Langford, B., Lin, C., Lewis, A. C., Li, J., Li, W., Liu, H., Liu, J., Loh, M., Lu, K., Lucarelli, F., Mann, G., McFiggans, G., Miller, M. R., Mills, G., Monk, P., Nemitz, E., O'Connor, F., Ouyang, B., Palmer, P. I., Percival, C., Popoola, O., Reeves, C., Rickard, A. R., Shao, L., Shi, G., Spracklen, D., Stevenson, D., Sun, Y., Sun, Z., Tao, S., Tong, S., Wang, Q., Wang, W., Wang, X., Wang, X., Wang, Z., Wei, L., Whalley, L., Wu, X., Wu, Z., Xie, P., Yang, F., Zhang, Q., Zhang, Y., Zhang, Y., and Zheng, M.: Introduction to the special issue “In-depth study of air pollution sources and processes within Beijing and its surrounding region (APHH-Beijing)”, Atmos. Chem. Phys., 19, 7519-7546, 10.5194/acp-19-7519-2019, 2019.

Silva, P. J., Liu, D.-Y., Noble, C. A., and Prather, K. A.: Size and Chemical Characterization of Individual Particles Resulting from Biomass Burning of Local Southern California Species, Environ. Sci. Technol., 33, 3068-3076, 10.1021/es980544p, 1999.

Silva, P. J., Carlin, R. A., and Prather, K. A.: Single particle analysis of suspended soil dust from Southern California, Atmos Environ, 34, 1811-1820, 10.1016/S1352-2310(99)00338-6, 2000.

Sodeman, D. A., Toner, S. M., and Prather, K. A.: Determination of single particle mass spectral signatures from light-duty vehicle emissions, Environ. Sci. Technol., 39, 4569-4580, 10.1021/es0489947, 2005.

Sullivan, R. C., Guazzotti, S. A., Sodeman, D. A., Tang, Y., Carmichael, G. R., and Prather, K. A.: Mineral dust is a sink for chlorine in the marine boundary layer, Atmos. Environ., 41, 7166-7179, 10.1016/j.atmosenv.2007.05.047, 2007.

Sun, Y., Jiang, Q., Wang, Z., Fu, P., Li, J., Yang, T., and Yin, Y.: Investigation of the sources and evolution processes of severe haze pollution in Beijing in January 2013, J Geophys Res, 119, 4380-4398, 2014a.

Sun, Y., Jiang, Q., Wang, Z., Fu, P., Li, J., Yang, T., and Yin, Y.: Investigation of the sources and evolution processes of severe haze pollution in Beijing in January 2013, J. Geophys. Res. Atmos., 119, 4380-4398, 10.1002/2014jd021641, 2014b.

Sun, Y. L., Wang, Z. F., Fu, P. Q., Yang, T., Jiang, Q., Dong, H. B., Li, J., and Jia, J. J.: Aerosol composition, sources and processes during wintertime in Beijing, China, Atmos. Chem. Phys., 13, 4577-4592, 10.5194/acp-13-4577-2013, 2013.

Tao, S., Wang, X., Chen, H., Yang, X., Li, M., Li, L., and Zhou, Z.: Single particle analysis of ambient aerosols in Shanghai during the World Exposition, 2010: two case studies, Front Environ Sci En, 5, 391-401, 10.1007/s11783-011-0355-x, 2011.

669 Toner, S. M., Shields, L. G., Sodeman, D. A., and Prather, K. A.: Using mass spectral
670 source signatures to apportion exhaust particles from gasoline and diesel powered vehicles
671 in a freeway study using UF-ATOFMS, Atmos. Environ., 42, 568-581,
672 10.1016/j.atmosenv.2007.08.005, 2008.

673 Wang, G., Zhang, R., Gomez, M. E., Yang, L., Levy Zamora, M., Hu, M., Lin, Y., Peng,
674 J., Guo, S., Meng, J., Li, J., Cheng, C., Hu, T., Ren, Y., Wang, Y., Gao, J., Cao, J., An, Z.,
675 Zhou, W., Li, G., Wang, J., Tian, P., Marrero-Ortiz, W., Secrest, J., Du, Z., Zheng, J.,
676 Shang, D., Zeng, L., Shao, M., Wang, W., Huang, Y., Wang, Y., Zhu, Y., Li, Y., Hu, J.,
677 Pan, B., Cai, L., Cheng, Y., Ji, Y., Zhang, F., Rosenfeld, D., Liss, P. S., Duce, R. A., Kolb,
678 C. E., and Molina, M. J.: Persistent sulfate formation from London Fog to Chinese haze,
679 Proc. Natl. Acad. Sci. U.S.A., 113, 13630-13635, 10.1073/pnas.1616540113, 2016.

680 Wang, H., Zhu, B., Zhang, Z., An, J., and Shen, L.: Mixing state of individual carbonaceous
681 particles during a severe haze episode in January 2013, Nanjing, China, Particuology, 20,
682 16-23, 10.1016/j.partic.2014.06.013, 2015.

683 Wang, H., Lu, K., Chen, X., Zhu, Q., Chen, Q., Guo, S., Jiang, M., Li, X., Shang, D., Tan,
684 Z., Wu, Y., Wu, Z., Zou, Q., Zheng, Y., Zeng, L., Zhu, T., Hu, M., and Zhang, Y.: High
685 N2O5 Concentrations Observed in Urban Beijing: Implications of a Large Nitrate
686 Formation Pathway, Environ. Sci. Technol. Lett., 4, 416-420, 10.1021/acs.estlett.7b00341,
687 2017.

688 Wang, J., Liu, D., Ge, X., Wu, Y., Shen, F., Chen, M., Zhao, J., Xie, C., Wang, Q., Xu, W.,
689 Zhang, J., Hu, J., Allan, J., Joshi, R., Fu, P., Coe, H., and Sun, Y.: Characterization of black
690 carbon-containing fine particles in Beijing during wintertime, Atmos. Chem. Phys., 19,
691 447-458, 10.5194/acp-19-447-2019, 2019.

692 Wang, P., Pan, B., Li, H., Huang, Y., Dong, X., Ai, F., Liu, L., Wu, M., and Xing, B.: The
693 Overlooked Occurrence of Environmentally Persistent Free Radicals in an Area with Low-
694 Rank Coal Burning, Xuanwei, China, Environ. Sci. Technol., 52, 1054-1061,
695 10.1021/acs.est.7b05453, 2018.

696 Xie, C., Xu, W., Wang, J., Wang, Q., Liu, D., Tang, G., Chen, P., Du, W., Zhao, J., Zhang,
697 Y., Zhou, W., Han, T., Bian, Q., Li, J., Fu, P., Wang, Z., Ge, X., Allan, J., Coe, H., and
698 Sun, Y.: Vertical characterization of aerosol optical properties and brown carbon in winter
699 in urban Beijing, China, Atmos. Chem. Phys., 19, 165-179, 10.5194/acp-19-165-2019,
700 2019.

701 Xu, J., Li, M., Shi, G., Wang, H., Ma, X., Wu, J., Shi, X., and Feng, Y.: Mass spectra
702 features of biomass burning boiler and coal burning boiler emitted particles by single
703 particle aerosol mass spectrometer, Sci Total Environ, 598, 341-352,
704 https://doi.org/10.1016/j.scitotenv.2017.04.132, 2017.

705 Xu, J., Wang, H., Li, X., Li, Y., Wen, J., Zhang, J., Shi, X., Li, M., Wang, W., Shi, G., and
706 Feng, Y.: Refined source apportionment of coal combustion sources by using single
707 particle mass spectrometry, Sci. Total Environ., 627, 633-646,
708 10.1016/j.scitotenv.2018.01.269, 2018.

709 Xu, W. Q., Sun, Y. L., Chen, C., Du, W., Han, T. T., Wang, Q. Q., Fu, P. Q., Wang, Z. F.,
710 Zhao, X. J., Zhou, L. B., Ji, D. S., Wang, P. C., and Worsnop, D. R.: Aerosol composition,
711 oxidation properties, and sources in Beijing: results from the 2014 Asia-Pacific Economic
712 Cooperation summit study, Atmos. Chem. Phys., 15, 13681-13698, 10.5194/acp-15-
713 13681-2015, 2015.

714 Zhai, J., Wang, X., Li, J., Xu, T., Chen, H., Yang, X., and Chen, J.: Thermal desorption
715 single particle mass spectrometry of ambient aerosol in Shanghai, Atmos. Environ., 123,
716 407-414, 10.1016/j.atmosenv.2015.09.001, 2015.

717 Zhai, S., An, X., Zhao, T., Sun, Z., Hou, Q., and Wang, C.: Detecting critical $PM_{2.5}$
718 emission sources and their contributions to a heavy haze episode in Beijing, China by using
719 an adjoint model, Atmospheric Chemistry and Physics Discussions, 2016, 1-20,
720 10.5194/acp-2016-911, 2016.

721 Zhang, R., Wang, G., Guo, S., Zamora, M. L., Ying, Q., Lin, Y., Wang, W., Hu, M., and
722 Wang, Y.: Formation of urban fine particulate matter, Chem. Rev., 115, 3803-3855,
723 10.1021/acs.chemrev.5b00067, 2015.

724 Zhao, J., Qiu, Y., Zhou, W., Xu, W., Wang, J., Zhang, Y., Li, L., Xie, C., Wang, Q., Du,
725 W., Worsnop, D. R., Canagaratna, M. R., Zhou, L., Ge, X., Fu, P., Li, J., Wang, Z.,
726 Donahue, N. M., and Sun, Y.: Organic Aerosol Processing During Winter Severe Haze
727 Episodes in Beijing, J. Geophys. Res. Atmos., 124, 10248-10263, 10.1029/2019jd030832,
728 2019.

729 Zheng, M., Yan, C. Q., Wang, S. X., He, K. B., and Zhang, Y. H.: Understanding PM2.5
730 sources in China: challenges and perspectives, Natl Sci Rev, 4, 801-803,
731 10.1093/nsr/nwx129, 2017.

732